Short-Time-Scale Thermal Mapping of Microdevices Using a Scanning Thermoreflectance Technique

Y. S. Ju
Graduate Student Researcher.
Student Mem. ASME

K. E. Goodson
Assistant Professor.
Assoc. Mem. ASME
e-mail: goodson@vk.stanford.edu

Department of Mechanical Engineering,
Stanford University, CA 94305-3030

The performance and reliability of microdevices can be strongly influenced by the peak temperature rise and spatial temperature distribution during brief electrical overstress (EOS) phenomena, which can occur at sub-microsecond time scales. The present study investigates short-time-scale laser reflectance thermometry of microdevices by examining the impact of passivation overlayers on the thermoreflectance signal and by demonstrating a calibration method suitable for metallization. This manuscript also describes a scanning laser thermometry facility that captures temperature fields in microdevices with 10 ns temporal resolution and 1 μm spatial resolution. The facility combines scanning laser optics with electrical stressing capability to allow simultaneous interrogation of the thermal and electrical behavior of devices. Data show the transient temperature distribution along the drift region of silicon-on-insulator (SOI) power transistors and along metal interconnects subjected to brief electrical stresses. The theory and experimental capability developed in this study are useful for studying short-time-scale thermal phenomena in microdevices and verifying models employed for their simulation.

1 Introduction

Many figures of merit of microdevices are influenced by transient thermal phenomena. Changes in the electrical behavior of semiconductor devices can result from self-heating, which occurs as a by-product of normal device operations. Transient self-heating is especially important for devices made from silicon-on-insulator substrates due to the large thermal resistance of the buried silicon dioxide layer, whose impact is most pronounced for rapid heating (Arnold, 1994). Semiconductor devices and interconnects can fail due to the temperature rise occurring on a time scale less than 1 μs during electrostatic discharge (ESD) (Amerasekera and Duvvury, 1995). Microdevices subjected to brief electrical stresses can experience large spatial temperature variations, which can vary with the duration of the stress and can induce highly localized failures (e.g., Ju and Goodson, 1997; Salome et al., 1997). In many microsensors and actuators, short-time-scale heating is required for proper functionality of the devices (Murguia and Bernstein, 1993; Chui et al., 1996). Thermometry techniques with high temporal and spatial resolution are needed to study the operation and failure of microdevices subjected to short-time-scale heating and to verify models used in device simulations.

Electrical thermometry methods use either electrically passive or active elements in an integrated circuit to obtain spatially averaged operating temperatures in devices. Temperature rises in interconnect structures subjected to sub-microsecond pulses have been obtained by measuring the temperature-dependent electrical resistance (e.g., Maloney and Khurana, 1985; Banerjee et al., 1996). Other investigators monitored temperature-sensitive electrical parameters (TSEPs), such as the emitter-base voltage of bipolar devices, to measure device temperatures (e.g., Arnold et al., 1994; Zweidinger et al., 1996). However, the spatial temperature distribution and the maximum temperature rise are often very difficult to obtain using the electrical methods (e.g., Leung et al., 1997). Another problem is that the achievable temporal resolution is limited by electrical transients in the case of TSEP-based thermometry and by electrical capacitive coupling between thermometers and devices in the case of the electrical-resistance thermometry.

Other thermometry techniques can obtain spatial temperature distributions in microdevices. Some optical techniques, such as liquid-crystal and fluorescence thermometry (Kolodner and Tyson, 1982), rely on a foreign film deposited on device surfaces. In these techniques, the characteristic time required for the changes in optical properties of the films restricts the achievable temporal resolution. The characteristic time for cholesteric liquid crystals is a few milliseconds (Fergason, 1968) and that for the EuTTA film used in fluorescence thermometry is around 100 μs as estimated from its fluorescence decay time (Kolodner and Tyson, 1983). The temporal resolution is ultimately limited by the thermal diffusion time across passivation layers present in many microdevices to the order of a few microseconds. Thermometry techniques based on scanning atomic force microscopy (AFM) can map temperature distributions with potential spatial resolution below 100 nm. This technique has been particularly successful at mapping steady-state temperature distributions in field-effect transistors and in semiconductor lasers (e.g., Majumdar et al., 1995). The temporal resolution of AFM-based techniques is diminished by the time lag resulting from thermal diffusion across passivation and into the probe tip as well as that associated with electrical capacitive and inductive coupling.

Infrared thermography has been used for failure studies of integrated circuit elements (e.g., Bennett and Briles, 1989; Kondo and Hinode, 1995). This technique requires careful calibration of the emissivity, which depends strongly on the surface topography and the wavelength. The optical interferometry technique (Martin and Wickramasinghe, 1987; Claeys et al., 1993) probes surface displacements due to thermal expansion to obtain temperature fields. This technique requires accurate knowledge of the relationship between local surface displace-

Contributed by the Heat Transfer Division and presented at the National Heat Transfer Conference, Houston, Texas, August 3–5, 1996. Manuscript received by the Heat Transfer Division April 21, 1997; revision received January 23, 1998. Keywords: Conduction, Measurement Techniques, Transient and Unsteady Heat Transfer. Associate Technical Editor: M. F. Modest.

ments and the temperature field, and is thus difficult to apply to semiconductor devices made of composite structures of materials with very different thermal expansion coefficients. Micro-Raman spectroscopy has been used for thermometry (Ostermeir et al., 1992). This approach is time-consuming and an application to transient measurements has not been reported.

The thermoreflectance technique is based on the temperature dependence of the optical reflectance (e.g., Cardona, 1969; Rosei and Lynch, 1972). This technique is promising for rapid thermal mapping of microdevices due to the temporal resolution better than 1 ns that has already been demonstrated on flat metal surfaces. Also promising is the opportunity to use radiation wavelengths for which most passivation layers are transparent. Several researchers employed the thermoreflectance thermometry technique to map the steady-state temperature distributions in semiconductor lasers (Epperlein, 1993; Mansanares et al., 1994) and the temperature distributions in interconnects and resistors (Claeys et al., 1993; Quintard et al., 1996). The short-time-scale thermometry of transistors and interconnects in integrated circuits subjected to brief electrical stresses, however, has received little attention. Another problem is that the development of calibration methods suitable for microdevices has not been properly addressed. The importance of accurate calibration grows with the application to integrated circuits, whose surfaces have optical properties that are not well characterized and can vary depending on the processing details.

In the present manuscript, we provide several results important for thermoreflectance thermometry of microdevices, including a theoretical study of the impact of passivation layers and a new calibration method. The passivation layers can strongly influence thermoreflectance signals due to the interference among multiply reflected beams, which is investigated here using thin film optics. The calibration method developed in this study uses electrical heating and thermometry in microstructures fabricated under the same processing conditions as the devices of interest. This work also develops a thermoreflectance thermometry facility that combines scanning laser optics with electrical stressing capability, which allows simultaneous investigation of thermal as well as electrical characteristics of microdevices. The facility achieves temporal resolution near 10 ns, which is limited by the bandwidth of the electrical measurement system, and spatial resolution near 1 μm, which is limited by the diffraction of a probe laser beam. The theory and experimental facility are used to obtain and interpret data for SOI power transistors and for interconnect structures.

2 Thermoreflectance Thermometry of Microdevices

A parameter characterizing the thermoreflectance phenomenon is denoted by C_{TR}, which is defined as the relative change in the reflectance per unit change in temperature. In this section we discuss various issues related to the thermoreflectance thermometry of microdevices, including the theoretical and experimental determination of thermoreflectance coefficients. The theoretical understanding and the calibration technique developed here are used in the design of subsequent experiments and the interpretation of experimental results.

2.1 Thermoreflectance Coefficient and Its Calibration. The previous thermoreflectance thermometry studies used C_{TR} from either theoretical predictions or existing experimental data on bulk samples or films, whose fabrication processes did not necessarily match those of actual samples tested. This is not appropriate for integrated circuits, whose surface materials, including passivation materials and various metal alloys, have optical properties that can vary with the processing conditions (e.g., Pliskin, 1977). Additional complications can arise for the case of semiconductors when they are part of an electrically active region of microdevices due to optoelectric effects. However, this issue will not be pursued further in this study, which performs thermometry using light–metal interactions.

Most films found in integrated circuits have relatively smooth surfaces with roughness smaller than the typical wavelength of the probe beam used in the thermoreflectance thermometry. The reflectance, in this case, can be expressed as a product of a surface-dependent quantity and a material-dependent quantity (Stagg and Charalampoulos, 1991). The thermoreflectance coefficient, defined in terms of the relative change in the reflectance, can therefore be modeled to first order as independent of the surface roughness.

Two different calibration methods for thermoreflectance coefficients can be used, one using an external temperature controller and the other employing microfabricated structures. In the first method, the temperature of a sample is controlled externally while variations in its reflectance are measured (e.g., Qiu et al., 1993). This approach has the advantage of a relatively simple experimental setup and is employed in the calibration of the power transistor structures studied in Section 3.2. Detailed discussion of the method is provided in that section. This method is difficult to apply when a sample or a film of interest has a small surface area. Thermal expansion of a sample–heater assembly can lead to systematic errors for an optical system with a high numerical aperture and a shallow focal depth. This problem can be remedied by localizing the heating, which strongly diminishes the thermally induced deflection of the surface. An example of this approach is to use a microstructure made of a film of interest both as a heater and as a thermometer.

Ju and Goodson (1997) performed calibration studies on long microfabricated metal lines, which are very nearly isothermal when subjected to electrical heating pulses. The temperature

Nomenclature

C = heat capacity per unit volume, J m^{-3} K^{-1}
C_{TR} = thermoreflectance coefficient, K^{-1}
d = thickness of a layer, m
k = thermal conductivity, W m^{-1} K^{-1}
k_{base} = imaginary part of the complex index of refraction of base material
$k_{T,Al}$ = temperature derivative of the imaginary part of index of refraction of aluminum, K^{-1}
L = overlayer thickness, m
n_{air} = index of refraction of air
$\tilde{n}_{base}$ = complex index of refraction of base material = $n_{base} - ik_{base}$
n_{base} = real part of the complex index of refraction of base material
n_{over} = index of refraction of an overlayer material
$n_{T,Al}$ = temperature derivative of the real part of the index of refraction of aluminum, K^{-1}
$n_{T,SiO2}$ = temperature derivative of the index of refraction of a silicon dioxide overlayer, K^{-1}
R = reflectance
r, r_1, r_2 = reflection amplitude coefficients
t = time after pulse initiation, s
x = coordinate along interconnect structures, m
y = coordinate along drift regions of power transistors, m
λ = wavelength in vacuum of probe laser, m

Subscripts

base = property of base material
BO = dimension of the buried silicon-dioxide layer in SOI power transistors
over = property or dimension of overlayer
s = dimension of silicon device layer in SOI power transistors

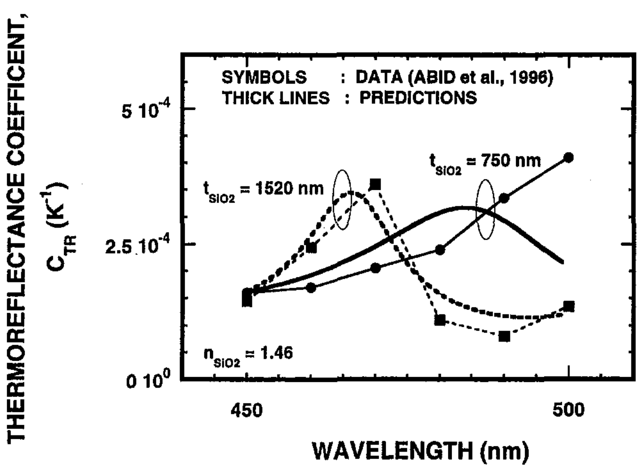

Fig. 1 Wavelength dependence of the thermoreflectance coefficient of silicon with silicon-dioxide overlayers. The predictions take into account the interference among multiply reflected beams.

derivative of the electrical resistance of the metal line was calibrated using a temperature-controlled wafer holder. The thermoreflectance coefficient was obtained by comparing the changes in the surface reflectance with those in the electrical resistance while subjecting the lines to electrical heating pulses. This method is ideally suited for the thermometry of interconnects and can also be applied to the thermometry of metallized portions of microdevices and doped semiconducting regions by microfabricating lines with the same material composition and fabrication techniques. This calibration method is employed in the thermal mapping of interconnect structures in the present study.

2.2 Impact of Overlying Passivation on the Thermoreflectance Signal. For a sample film with an overlying dielectric layer, whose thickness is typically of the order of the wavelength of a probe beam, the impact of the overlayer on the thermoreflectance signal must be considered. Interference among multiply reflected beams alters the optical reflectance and also influences the thermoreflectance signal in a manner that is sensitive to its thickness, the wavelength of a probe beam, and the optical properties of both the overlayer and the underlying base material. The presence of a silicon dioxide layer has been observed to alter the surface reflectance of silicon and its temperature dependence (e.g., Friedrich et al., 1991; Quintard et al., 1996).

The present study uses the theory of thin-film optics (Siegel and Howell, 1992) to predict the impact of passivation layers and to draw conclusions about the resulting uncertainty in thermoreflectance thermometry of underlying opaque layers. For normal incidence, the surface reflectance, R, is related to the indices of refraction, $\tilde{n}_{\text{base}}$ and n_{over}, and the thickness of the overlayer, L,

$$R = \left| \frac{r_1 + r_2 \exp(-i4\pi n_{\text{over}} L/\lambda)}{1 + r_1 r_2 \exp(-i4\pi n_{\text{over}} L/\lambda)} \right|^2 \quad (1)$$

The amplitude reflection coefficients r_1 and r_2 are

$$r_1 = \frac{n_{\text{air}} - n_{\text{over}}}{n_{\text{air}} + n_{\text{over}}} \quad (2)$$

$$r_2 = \frac{n_{\text{over}} - \tilde{n}_{\text{base}}}{n_{\text{over}} + \tilde{n}_{\text{base}}} \quad (3)$$

The dielectric overlayer is assumed to be transparent at the probe beam wavelength and its absorption coefficient is neglected. The thermoreflectance coefficient, C_{TR}, is given by

$$C_{TR} = \frac{1}{R}\frac{dR}{dT} \quad (4)$$

and can be calculated if the temperature dependence of the indices of refraction of a given material is known.

Equations (1)–(3) are applied to passivated silicon samples, whose thermoreflectance coefficients were measured by Abid et al. (1996) for several different probe beam wavelengths. Silicon is chosen since its optical properties are very well characterized over large temperature and wavelength ranges and hence the comparison of the prediction with the data is most meaningful. The experimental data of Jellison and Modine (1982a, b) and Jellison and Burke (1986) are used in the present calculations. The index of refraction of silicon dioxide is assumed to be constant at the value of 1.46 unless otherwise specified. Figure 1 compares the experimental data with the predictions for two different thicknesses of the silicon dioxide layers. Although the thermoreflectance coefficient of silicon is nearly constant over the wavelength range examined, large variations in C_{TR} result from the interference effects. The predictions agree reasonably well with the data except for the 750 nm oxide case near the wavelength of 500 nm. The discrepancy can result from several different sources, including the uncertainties in the indices of refraction of silicon and silicon dioxide as well as those in the thickness of the overlayer.

Another source of error, which has been neglected in the previous studies, is associated with the temperature dependence of the index of refraction of silicon dioxide. The magnitude of the temperature derivative of the index of refraction, $n_{T,\text{SiO2}}$, is comparable to 10^{-5} K^{-1} (van der Meulen and Hien, 1974; Guidotti and Wilman, 1992). However, this temperature dependence can have a significant influence on the thermoreflectance signal. If n_{over} is assumed to be independent of temperature, both the reflectance, R, and its temperature derivative are periodic functions of the overlayer thickness L. If, in contrast, $n_{T,\text{over}}$ is nonzero, phase differences between the oscillations of R and dR/dT exist as illustrated in Fig. 2 for the case of a silicon-dioxide passivated silicon sample. The variations in dR/dT are not periodic and the thermoreflectance coefficient oscillates with growing amplitude as L increases. The thermal expansion of the silicon dioxide layer is not considered explicitly but, since the thickness of the overlayer appears only as a product with n_{over}, its influence is contained in $n_{T,\text{over}}$.

The influence of the temperature dependence of n_{over} on the thermoreflectance signal has an additional implication for the transient thermometry of passivated microdevices. When the thermal diffusion time across the passivation overlayer is larger

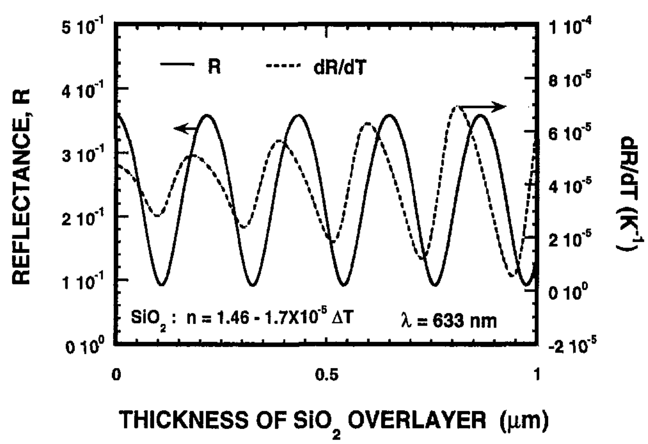

Fig. 2 The reflectance and its temperature derivative as functions of the thickness of an overlying silicon-dioxide layer for the case of silicon base material. The temperature derivative of the index of refraction of silicon dioxide, $n_{T,\text{SiO2}}$, is taken from previous research.

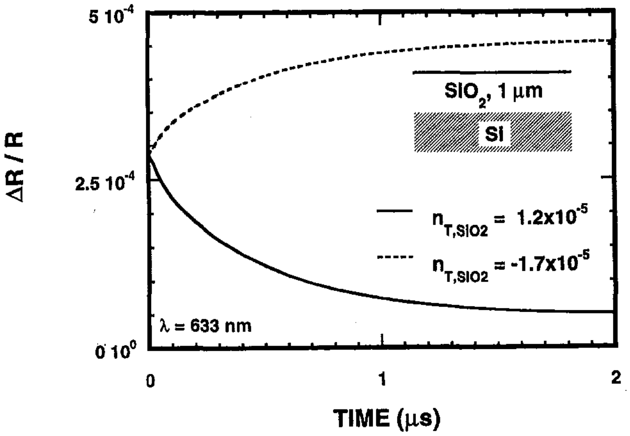

Fig. 3 Time evolution of thermoreflectance signals of a silicon sample covered with a 1-μm-thick silicon-dioxide layer, which results from the time variation of temperature fields within the overlayer. The temperature of the silicon sample undergoes a step change at time $t = 0$ and remains constant thereafter.

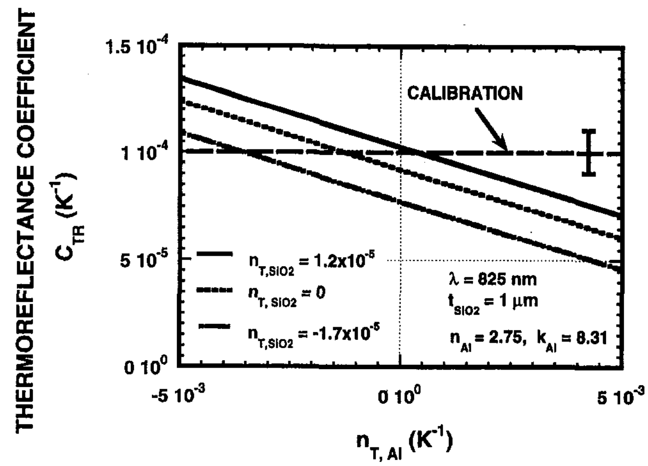

Fig. 4 Impact of uncertainties in the temperature dependence of the index of refraction of aluminum on the thermoreflectance coefficient of an aluminum layer with a 1-μm-thick silicon-dioxide overlayer. The calibration result, shown as a horizontal line, is a guide for comparison with the calculations. The vertical bar represents the experimental uncertainty limit and its horizontal location is immaterial.

than or comparable to the measurement time scale, the variation of the thermoreflectance signal resulting from the temperature distribution within the overlayer must be taken into account. To illustrate this point, the time evolution of a thermoreflectance signal is calculated for a silicon sample that experiences a step change in temperature. The silicon sample is covered with a silicon dioxide layer of thickness 1 μm, which is modeled optically as consisting of parallel sublayers of uniform thickness. For the optical analysis, each sublayer is assumed to be isothermal and its temperature is obtained by solving the transient one-dimensional heat conduction equation. An adiabatic boundary condition is applied to the outer surface of the oxide layer. The temperature of the silicon sample is increased by a step function at time $t = 0$.

The reflectance of a stratified multilayer can be calculated using the transmission matrix method (Knittl, 1976). Figure 3 shows the calculated results of the relative change in the surface reflectance as a function of time for two different values of $n_{T,\mathrm{SiO2}}$ taken from the previously cited references. The thermoreflectance signal tends toward the values corresponding to the case where the entire overlayer is at the substrate temperature. The difference between the two steady-state values is large for the particular case shown here and depends on L and $n_{T,\mathrm{over}}$ as well as the optical properties of the base material. The error resulting from this time-varying thermoreflectance signal would be less severe since the assumed step change in the substrate temperature tends to exaggerate its impact. When the thermoreflectance coefficient is very sensitive to $n_{T,\mathrm{over}}$ and the time scale of interest is less than the thermal diffusion time across an overlayer, however, much care is required to interpret the thermoreflectance signal properly. Careful selection of the probe beam wavelength can help overcome difficulties related to the high sensitivity of thermoreflectance signals to the overlayer (e.g., Epperlein, 1993; Abid et al., 1996).

Similar calculations can be performed for a metal base material. Aluminum is chosen as a base material here and is used for the transistor structures studied in Section 3.2. The wavelength of the probe beam is chosen to be 825 nm, at which the previously measured thermoreflectance coefficient is maximum within the visible and near-infrared wavelength range (Decker and Hodgkin, 1981). The present calculation uses a complex refractive index of the form (Smith et al., 1985)

$$n_{\mathrm{base}} = (2.75 + n_{T,Al}\Delta T) - i(8.31 + k_{T,Al}\Delta T). \quad (5)$$

The two parameters, $n_{T,Al}$ and $k_{T,Al}$, are not available in the literature to the best of our knowledge and cannot be determined uniquely from the index of refraction and the thermoreflectance coefficient of bare aluminum at a single temperature (e.g., Miklós and Lörincz, 1988). A parametric study is performed, where C_{TR} of a passivated aluminum film is calculated as a function of $n_{T,Al}$ and is shown in Fig. 4. For each value of $n_{T,Al}$, the corresponding value of $k_{T,Al}$ is first obtained by requiring the resulting C_{TR} in the absence of an overlayer to be the experimentally measured value. The thickness of the silicon-dioxide layer is fixed at 1 μm in the calculations, which is the thickness used in the later experiments. The results indicate that the thermoreflectance coefficient is much less sensitive to $n_{T,\mathrm{SiO2}}$ than is the case for passivated silicon samples. The calibration result of the present study is also shown in Fig. 4 for comparison. Further discussion on the thermoreflectance coefficient of a passivated aluminum layer and its calibration are provided in Section 3.2 in connection with the thermometry of transistor structures.

3 Measurement Examples

This section describes the experimental apparatus developed in this study for high temporal and spatial resolution thermometry of microdevices and presents calibration results and data for SOI power transistors and metal interconnect structures.

3.1 Experimental Apparatus. The present study develops the experimental facility shown in Fig. 5, which integrates scanning laser diagnostics and electrical probing and thus allows

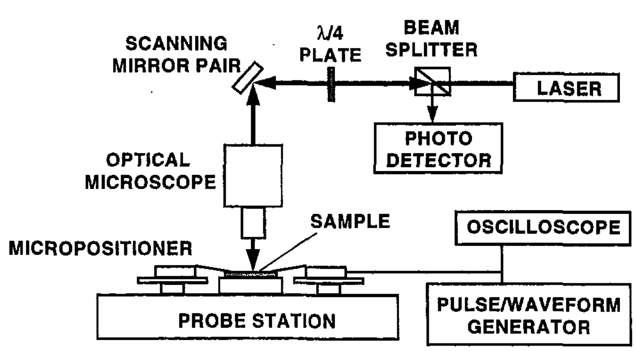

Fig. 5 Schematic of the scanning laser-reflectance thermometry facility developed in the present study. A probe laser beam is focused down to the diffraction limit by an optical microscope and scanned over a sample surface using a pair of scanning mirrors.

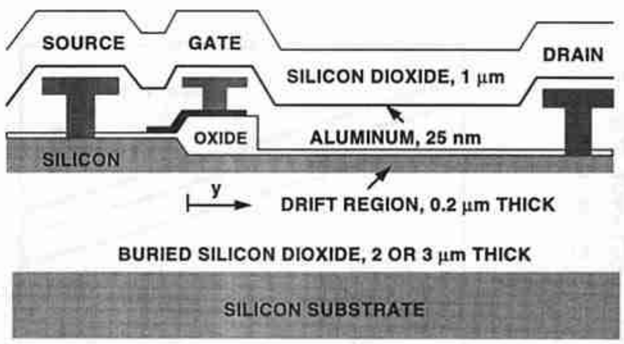

Fig. 6 Cross section of the silicon-on-insulator (SOI) high-voltage transistor structure studied in the present work. A thin aluminum layer of thickness 25 nm is deposited between silicon-dioxide passivation layers for measurement purposes. Temperature distributions along the drift region are measured using the facility shown in Fig. 5.

simultaneous investigation of thermal and electrical behavior of microdevices. A laser diode system with a single-element glass aspheric focusing lens and astigmatic correction optics is used. The output beam from the diode laser system has a Gaussian intensity profile with the beam divergence angle of 0.14 mrad. Radiation from the laser diode system is coupled into an optical microscope and focused to a diameter near the wavelength using microscope objective lenses with numerical aperture as high as 0.9. The wavelength of the laser diode used in the present study is 825 nm. The probe laser focus is scanned over the wafer surface using a pair of galvanometrically actuated mirrors that rotate about orthogonal axes while the semiconductor device and the electrical probes remain stationary. This feature allows the use of standard microprobes, facilitating wafer-level device characterization. A polarization cube and a quarter-wave plate separate the incident and reflected probe beam paths. Laser power fluctuations are subtracted using a reference beam drawn by a beam splitter. The radiation powers are captured using photodiodes with 500 MHz bandwidth and a digital oscilloscope with 1 GHz sampling frequency. The temporal resolution achievable in this setup is near 10 ns and the spatial resolution is limited by the diffraction of a probe beam to the order of its wavelength. The current setup allows the direct observation of sample surfaces during the measurements either through an eyepiece or a CCD camera. Using a calibration structure, the size and location of the focused beam spot can be measured and monitored during the scan process.

3.2 Thermometry of SOI High-Voltage Transistors. The thermoreflectance thermometry technique is applied to silicon-on-insulator (SOI) power transistors, which are designed to block high-voltages in power circuitry (Ju et al., 1997). A schematic of the transistor structure used in the experiments is shown in Fig. 6. To assist with the thermometry, an aluminum layer is sputtered within the surface oxide. The thickness of the aluminum layer is 25 nm, which is larger than the optical penetration depth of 8 nm at the probe beam wavelength. It therefore strongly reduces interaction between the radiation and the transistor and precisely defines the vertical location at which temperature is measured. The length of the drift region, over which the aluminum layer is deposited, is 40 μm.

The numerical aperture of the microscope objective lens used for the measurements is 0.5. The probe beam power is less than 1 mW. The temperature rise due to laser heating is estimated to be small since the conduction cooling through the substrate, which is augmented by the lateral spreading of heat in the metal film, is substantial. For values on the absorbed laser power as high as 0.1 mW, the estimated laser-induced temperature rise in the 25-nm-thick aluminum layer is less than 10 K. Since the present technique measures changes in temperature rather than its absolute magnitude, the steady-state temperature field does not directly influence the measurements. When the laser-induced heating is significant, however, it can alter device characteristics and thereby indirectly affect the results. The impact of laser heating on the measurements is examined experimentally by varying the incident probe beam power and also the focused beam spot size. There are no observable variations either in the measured temperature rises or in the electrical characteristics of the devices.

The calibration for the transistor structures is performed using the transistor structures themselves. The silicon wafer containing the transistors is fixed to a temperature-controllable hot-chuck, which is made of copper, by means of air suction. The changes in the surface reflectance are monitored while inducing periodic variations in the wafer temperature. The area of the transistor region, over which the aluminum layer is deposited, is large enough to allow the use of an optical system with a large depth of focus. This avoids error resulting from the thermal expansion of the calibration system. To verify the calibration, a control wafer is prepared using micro-fabrication processes identical to those for the transistor structures, but with the aluminum layer over the entire wafer. By removing the need for focusing optics, the impact of the thermal expansion of the calibration system can be eliminated. The two calibration results agree well within the uncertainty limit.

The area of a focused Gaussian beam varies as the beam travels through a medium in a manner that depends on the wavelength and the waist size of the beam. The spatial regions occupied by the multiply reflected beams do not exactly coincide with each other, which can influence interference among them and ultimately the thermoreflectance coefficient. The impact of the beam area variation, however, is not expected to be significant for the present measurements, where the reflected beam is collected through the lens used to focus the beam. Most of the collected light come from those portions of the multiply reflected beams that spatially overlap the beam waist. The small reflectance at the interface between the oxide layer and the ambient air, together with the fact that the Rayleigh range is over 5 μm for the present case, further reduces the impact. The insignificance of the beam area variation is verified experimentally using a transistor structure similar to the one shown in Fig. 6. The electrical resistivity and hence the local heat generation rate are made to be uniform along the drift region for this structure, which results in a temperature field that is uniform over a large portion of the drift region. Temperature measurements are performed using microscope objective lenses with numerical apertures of 0.1, 0.2, and 0.5, while subjecting the device to identical electrical stressing conditions. The results for the three lenses with very different beam waist sizes vary by less than 5 percent.

In Section 2.2, it is noted that the thermoreflectance coefficient can vary with time due to the temperature dependence of the index of refraction of the dielectric passivation layer. Parametric study performed on the aluminum layer indicates that for a reasonable range of values of the parameters involved, the resulting error is not significant. For times greater than the thermal diffusion time across the overlying oxide layer, which is near 1 μs in this case, the temperature variation within the passivation overlayer and its influence on the thermoreflectance signal can be neglected.

During the thermometry, periodic voltage pulses of duration near 30 μs and magnitude near 30 V are applied to the drain. The duration of the pulse is chosen such that the influence of the buried oxide layer on the temperature rise can be examined over a large duration. The duty cycle of the periodic pulses is less than 0.01 to ensure complete cooling of the devices between successive heating pulses. The gate of the transistor is positively biased at 12 V and the source is grounded. At each scan point, the periodic temperature rise is acquired as a function of time after pulse initiation. Once these data are obtained for the entire

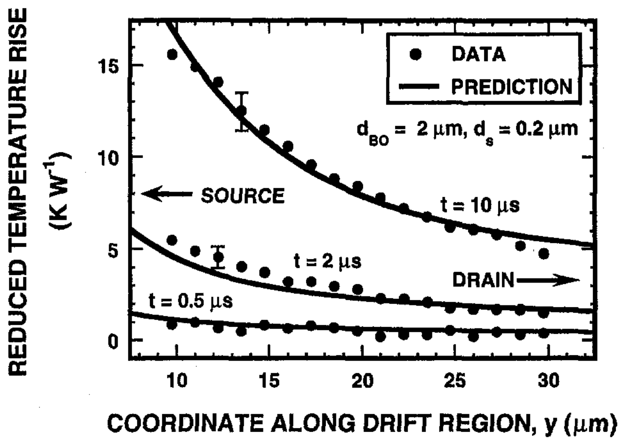

Fig. 7 Temperature distributions along the drift region of the transistors subjected to current pulses of duration 30 μs. The reduced temperature rise is the temperature rise per unit power dissipated in the device. Spatial variations in the impurity concentration lead to nonuniform temperature distributions.

sample surface, the spatial temperature-rise map can be extracted at any time.

A major source of noise in the current setup is the diode laser, which is sensitive to the back reflection and the environmental conditions. The photo-detector and signal amplifier contribute additional noise. The temperature resolution of 0.1 K is achieved by averaging signals 256 times. The relative uncertainty in the absolute value of the measured temperature rise is dominated by that in the calibration coefficient, C_{TR}, which is estimated to be 10 percent. Being independent of the calibration coefficient, the uncertainty in the ratio of temperature rises at different locations or at different times is much smaller, estimated to be 5 percent.

Practical limitations on the actual temporal and spatial resolution are imposed by the measurement structure due to the heat conduction within the aluminum and the passivation layers. Spatial resolution limit of 1 μm, which is not more restrictive than that due to the diffraction of the incident probe laser beam, and temporal resolution of 0.5 μs are estimated (Ju et al., 1997). These practical limitations on the resolution can be removed for the thermometry of interconnects and metallized regions of microdevices, which do not require any structure modifications.

Figure 7 shows the temperature distribution measured along the drift region of the SOI transistor for varying times after the initiation of the heating pulse. Since the thermal diffusion time normal to the buried silicon dioxide is comparable to 5 μs, the data actually describe transient heat diffusion *within* the silicon dioxide surrounding the active region. The temperature rise increases with decreasing coordinate y due to the spatial variation of the phosphorous impurity concentration, which is used to improve voltage-blocking capability (Leung et al., 1997). Since the current density does not vary significantly within the drift region, the rate of heat generation is proportional to the local electrical resistivity, which decreases with increasing impurity concentration. Figure 7 includes the predictions based on numerical solutions to the transient, two-dimensional heat equation in the drift region and surrounding silicon dioxide. The simulation uses bulk resistivity data for phosphorus-doped silicon with concentration distribution that is consistent with the fabrication process. The thermal conductivity and heat capacity used for the calculations are 100 W m^{-1} K^{-1} and 1.66 $\times$ 10^6 J m^{-3} K^{-1} for silicon and 1.4 W m^{-1} K^{-1} and 1.65 $\times$ 10^6 J m^{-3} K^{-1} for silicon dioxide, respectively (Goodson et al., 1996). The thermal conductivity of the silicon device layers used, which is lower than the bulk value, takes into account the reduction in the thermal conductivity due to phonon-boundary scattering. The simulation assumes that the top boundary condition for the passivation is adiabatic, and the bottom boundary condition for the buried silicon dioxide is isothermal. These assumptions are justified by the extremely low convection and radiation heat losses to the ambient air and by the short time scale of the heating pulse, respectively. The shape and time dependence of the calculated temperature rise agree well with the data.

3.3 Interconnect Thermometry. The interconnect structures examined in this study are shown in Fig. 8. The metal lines are 4 μm wide and 0.5 μm thick and are deposited on the composite passivation layers consisting of silicon-dioxide and polymer layers. The interconnects are made of Al-Cu-Ti alloy with the electrical resistivity of 3.37 $\times$ 10^{-8} Ω m. The thermoreflectance coefficient of 5.5 $\times$ 10^{-4} K^{-1} is obtained using a nearby 2000-μm-long metal line both as a heater and an electrical resistance thermometer according to the method described in Section 2.4. The uncertainty in the absolute magnitude of temperature rises is again dominated by that in the calibration coefficient, which is estimated to be 10 percent. The numerical aperture of the lens is 0.9 and the incident probe beam power is less than 1 mW. The influence of the laser-induced heating is examined by varying the laser power and is found not to be significant. Due to the increased detector noise at short time scales and the small thermoreflectance coefficient, achieving resolution better than 1 K requires averaging of signals by more than 1024 times. This number could be reduced by employing a more stable laser, such as a gas laser, as a light source, by prefiltering high frequency noise components, and by performing post-processing of data.

Figure 9 compares the normalized shapes of the spatial temperature distributions along interconnects subjected to electrical heating pulses of duration 200 ns and 2 μs. The temperature distributions become more rounded with increasing time after the pulse initiation. This is because the interconnect ends are anchored near the initial temperature due to their proximity to the metal regions with larger width. At a given time t, the influence of the lower temperature end conditions propagates inward over a distance comparable to the heat diffusion length in metal. For the largest value of t, the data are relatively independent of x only within a small portion of the interior of the line. Shown also are the predicted spatial temperature profiles, which are obtained from a numerical heat conduction analysis in the metal. The cross-sectional temperature distribution of the metal at each location along the interconnect is assumed to be uniform and all the boundaries are assumed to be adiabatic. The influence of the underlying passivation layer on the lengthwise temperature profile is neglected, since its thermal conductivity is two orders of magnitude smaller than that of the metal.

For the pulse of duration 200 ns, the temperature rise at the middle portion of the interconnect can be simulated by solving

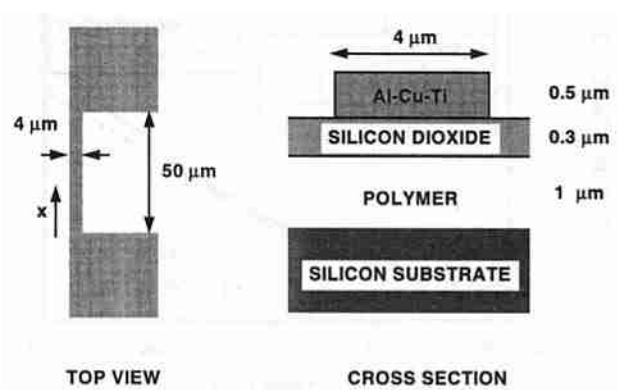

Fig. 8 Schematic of interconnect structures studied here. The interconnects are made of Al/Cu alloy and are separated from the silicon substrate by an underlying passivation layer. Electrical connections are made through two large area contact pads.

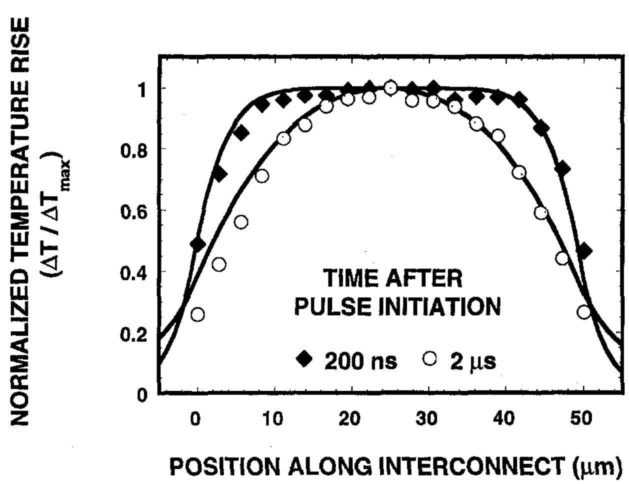

Fig. 9 Normalized temperature profiles along the interconnect structures subjected to brief electrical pulses of duration 200 ns and 2.5 μs. Solid lines are the predictions from the heat conduction analysis within the metals.

the transient two-dimensional heat conduction equation. Figure 10 plots the experimentally measured temperature rise and the predictions, which show good agreement up to the time after pulse initiation of 150 ns. The thermal boundary resistance resulting from the poor interface quality between the silicon dioxide and the polymer layer (Ju and Goodson, 1997) is believed to enhance temperature rises at later times. Numerical values of the thermal properties used for the simulations are shown in the figure. The time derivative of the temperature rise is small for short times after the pulse initiation due to the pulse rise time of 50 ns.

4 Summary and Conclusions

The performance and reliability of microdevices subjected to brief electrical stresses are strongly influenced by the presence of localized hot spots and regions with high temperature gradients, whose locations can vary with the time scales of electrical stresses. Concurrent electrical and thermal design are necessary to assure the optimal performance and reliability of these devices. Transient thermal mapping techniques can aid the design process by locating problematic regions and by providing quantitative information on temperature fields in microdevices.

The present work studies a scanning thermoreflectance technique, which is promising for transient thermal mapping of microdevices. The impact of passivation layers on the thermoreflectance coefficient is examined and a calibration technique suitable for integrated circuit elements is developed. This work shows that the proper interpretation of the thermoreflectance signal is necessary for the transient thermometry of passivated microdevices. A thermoreflectance thermometry facility combining scanning laser optics with electrical stressing capability is built and spatial resolution of 1 μm and temporal resolution near 10 ns are demonstrated.

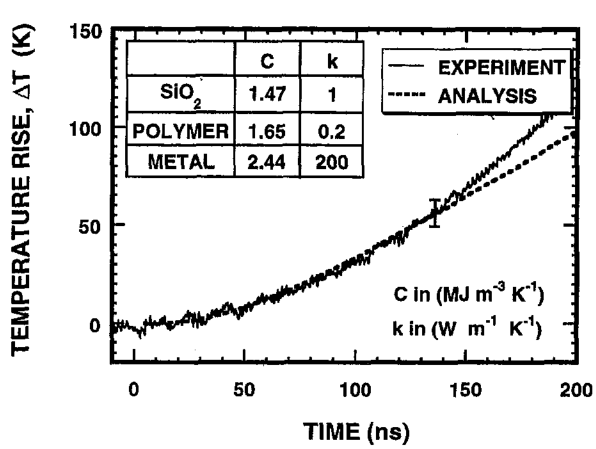

Fig. 10 Comparison of the experimentally measured time evolution of the temperature rise in the interconnect and the predictions based on the transient heat conduction equation

Acknowledgments

Y. S. J. acknowledges support from the member companies of the Center for Integrated Systems at Stanford University and Texas Instruments, Inc. K. E. G. acknowledges the ONR Young Investigator Award and support of the Semiconductor Research Corporation through contract No. 97-SJ-461. The SOI transistors were fabricated by Dr. Y.-K. Leung and Prof. S. S. Wong of Department of Electrical Engineering at Stanford University and the interconnect samples were provided by Intel Corporation. Y. S. J. appreciates the aid of Dr. O. W. Käding, W. Sabala, and L. Johal in building the experimental setup.

References

Abid, R., Miserey, F., and Mezroua, F.-Z., 1996, "Effet de la Température sur la Réflectivité du Silicium Oxydé: Détermination Expérimentale de la Sensibilité Relative; Application à la Mesure sans Contact de la Température à la Surface d'un Thyristor GTO en Commutation," *J. de Phys. III*, Vol. 6, pp. 279–300.

Amerasekera, A., and Duvvury, C., 1995, *ESD in Silicon Integrated Circuits*, Wiley, Chichester.

Arnold, E., 1994, "Silicon-on-Insulator Devices for High Voltage and Power IC Applications," *J. Electrochem. Soc.*, Vol. 141, pp. 1983–1988.

Arnold, E., Pein, H., and Herko, S. P., 1994, "Comparison of Self-Heating Effects in Bulk-Silicon and SOI High-Voltage Devices," *IEDM Technical Digest*, pp. 813–816.

Banerjee, K., Amerasekera, A., and Hu, C., 1996, "Characterization of VLSI Interconnect Heating and Failure under ESD Conditions," *Proc. Int. Reliab. Phys. Symp.*, pp. 237–245.

Bennett, G. A., and Briles, S. D., 1989, "Calibration Procedure Developed for IR Surface-Temperature Measurements," *IEEE Trans. Components, Hybrids and Manufacturing Technol.*, Vol. 12, pp. 690–695.

Cardona, M., 1969, "Modulation Spectroscopy," in: *Solid State Physics*, Suppl. 11, Seitz, F., Turnbull, D., and Ehrenreich, H., eds., Academic Press, New York.

Chui, B. W., Stowe, T. D., Ju, Y. S., Goodson, K. E., Kenny, T. W., Mamin, H. J., Terris, B. D., Ried, R. P., and Rugar, D., 1998, "Low-Stiffness Silicon Cantilevers With Integrated Heaters and Piezoresistive Sensors for High-Density AFM Thermomechanism Data Storage," *J. MEMS*, Vol. 7, pp. 69–78.

Claeys, W., Dilhaire, S., Quintard, V., Dom, J. P., and Danto, Y., 1993, "Thermoreflectance Optical Test Probe for the Measurement of Current-Induced Temperature Changes in Microelectronic Components," *Reliability Eng. Int.*, Vol. 9, pp. 303–308.

Decker, D. L., and Hodgkin, V. A., 1981, "Wavelength and Temperature Dependence of the Absolute Reflectance of Metals at Visible and Infrared Wavelengths," in: *National Bureau of Standards Special Publication*, NBS-SP-620, Washington, DC.

Eeseley, G. L., 1986, "Generation of Nonequilibrium Electron and Lattice Temperatures in Copper by Picosecond Laser Pulses," *Phys. Rev. B*, Vol. 33, pp. 2144–2151.

Epperlein, P.-W., 1993, "Micro-Temperature Measurements on Semiconductor Laser Mirrors by Reflectance Modulation: A Newly Developed Technique for Laser Characterization," *Jpn. J. Appl. Phys.*, Vol. 32, pp. 5514–5522.

Fergason, J. L., 1968, "Liquid Crystals in Nondestructive Testing," *Applied Optics*, Vol. 7, pp. 1729–1737.

Friedrich, K., Walther, H. G., and von Geisau, O. H., 1991, "A Method to Increase the Sensitivity of Temperature Measurements of Current-Carrying Microelectronic Components," *Rev. Sci. Instrum.*, Vol. 62, pp. 805–809.

Goodson, K. E., Flik, M. I., Su, L. T., and Antoniadis, D. A., 1995, "Prediction and Measurement of Temperature Fields in Silicon-on-Insulator Electronic Circuits," ASME Journal of Heat Transfer, Vol. 117, pp. 574–581.

Goodson, K. E., Ju, Y. S., Asheghi, M., Käding, O. W., Touzelbaev, M. N., Leung, Y.-K., and Wong, S. S., 1996, "Microscale Thermal Characterization of High-Power Silicon-on-Insulator Transistors," *Proc. 31st ASME National Heat Transfer Conference*, Vol. 5, pp. 1–9.

Guidotti, D., and Wilman, J. G., 1992, "Nulling Optical Bridge for Nonintrusive Temperature Measurements," *J. Vac. Sci. Technol. A*, Vol. 10, pp. 3184–3192.

Jellison, G. E., Jr., and Modine, F. A., 1982a, "Optical Absorption of Silicon Between 1.6 and 4.7 eV at Elevated Temperatures," *Appl. Phys. Lett.*, Vol. 41, pp. 180–182.

Jellison, G. E., Jr., and Modine, F. A., 1982b, "Optical Constants for Silicon at 300 and 10 K Determined from 1.64 to 4.73 eV by Ellipsometry," *J. Appl. Phys.*, Vol. 53, pp. 3745–3753.

Jellison, G. E., Jr., and Burke, H. H., 1986, "The Temperature Dependence of the Refractive Index of Silicon at Elevated Temperatures at Several Laser Wavelengths," *J. Appl. Phys.*, Vol. 60, pp. 841–843.

Ju, Y. S., Käding, O. W., Leung, Y. K., Wong, S. S., and Goodson, K. E., 1997, "Short-Timescale Thermal Mapping of Semiconductor Devices," *IEEE Electron Device Lett.*, Vol. 18, pp. 169–171.

Ju, Y. S., and Goodson, K. E., 1997, "Short-Timescale Thermal Mapping of Interconnects," *IEEE Proc. Int. Reliab. Phys. Symp.*, Denver, CO, pp. 320–324.

Knittl, Z., 1976, *Optics of Thin Films*, Wiley, London.

Kolodner, P., and Tyson, J. A., 1982, "Microscopic Fluorescent Imaging of Surface Temperature Profiles With 0.01 C Resolution," *Appl. Phys. Lett.*, Vol. 40, pp. 782–784.

Kolodner, P., and Tyson, J. A., 1983, "Remote Thermal Imaging With 0.7-μm Spatial Resolution Using Temperature-Dependent Fluorescent Thin Films," *Appl. Phys. Lett.*, Vol. 42, pp. 117–119.

Kondo, S., and Hinode, K., 1995, "High-Resolution Temperature Measurement of Void Dynamics Induced by Electromigration in Aluminum Metallization," *Appl. Phys. Lett.*, Vol. 67, pp. 1606–1608.

Leung, Y.-K., Kuehne, S. C., Huang, V. S. K., Nguyen, C. T., Paul, A. K., Plummer, J. D., and Wong, S. S., 1997, "Spatial Temperature Profiles Due to Nonuniform Self-Heating in LDMOS's in Thin SOI," *IEEE Electron Device Lett.*, Vol. 18, pp. 13–15.

Maloney, T. J., and Khurana, N., 1985, "Transmission Line Pulsing Techniques for Circuit Modeling of ESD Phenomena," *Proc. EOS/ESD Symp.*, pp. 49–54.

Mansanares, A. M., Roger, J. P., Fournier, D., and Boccara, A. C., 1994, "Temperature Field Determination of InGaAsP/InP Lasers by Photothermal Microscopy: Evidence for Weak Nonradiative Processes at the Facets," *Appl. Phys. Lett.*, Vol. 64, pp. 4–6.

Majumdar, A., Lai, J., Chandrachood, M., Nakabeppu, O., Wu, Y., and Shi, Z., 1995, "Thermal Imaging by Atomic Force Microscopy Using Thermocouple Cantilever Probes," *Rev. Sci. Instrum.*, Vol. 66, pp. 3584–3592.

Martin, Y., and Wickramasinghe, H. K., 1987, "Study of Dynamic Current Distribution in Logic Circuits by Joule Displacement Microscopy," *Appl. Phys. Lett.*, Vol. 50, pp. 167–168.

Miklós, A., and Lörincz, A., 1988, "Transient Thermoreflectance of Thin Metal Films in the Picosecond Regime," *J. Appl. Phys.*, Vol. 63, pp. 2391–2395.

Murguia, J. E., and Bernstein, J. B., 1993, "Short-time Failure of Metal Interconnect Caused by Current Pulses," *IEEE Electron Device Lett.*, Vol. 14, pp. 481–483.

Ostermeir, R., Brunner, K., Abstreiter, G., and Weber, W., 1992, "Temperature Distribution in Si-MOSFET's Studied by Micro Raman Spectroscopy," *IEEE Trans. Electron Devices*, Vol. 39, pp. 858–863.

Pliskin, W. A., 1977, "Comparison of Properties of Dielectric Films Deposited by Various Methods," *J. Vac. Sci. Technol.*, Vol. 14, pp. 1064–1081.

Quintard, V., Deboy, G., Dilhaire, S., Lewis, D., Phan, T., and Claeys, W., 1996, "Laser Beam Thermography of Circuits in the Particular Case of Passivated Semiconductors," *Microelectronic Engineering*, Vol. 31, pp. 291–298.

Qiu, T. Q., Grigoropoulos, C. P., and Tien, C. L., 1993, "Novel Technique for Noncontact and Microscale Temperature Measurements," *Experimental Heat Transfer*, Vol. 6, pp. 231–241.

Rosei, R., and Lynch, D. W., 1972, "Thermomodulation Spectra of Al, Au, and Cu," *Phys. Rev. B*, Vol. 5, pp. 3883–3893.

Salome, P., Leroux, C., Chante, J. P., Crevel, P., and Reimbold, G., 1997, "Study of the 3D Phenomenon During ESD Stresses in Deep Submicron CMOS Technologies Using a Photon Emission Tool," *IEEE Proc. Int. Reliab. Phys. Symp.*, Denver, CO, pp. 325–332.

Shirley, C. G., 1985, "Steady-State Temperature Profiles in Narrow Thin-Film Conductors," *J. Appl. Phys.*, Vol. 57, pp. 777–784.

Siegel, R., and Howell, J. R., 1992, *Thermal Radiation Heat Transfer*, Hemisphere Publishing Co., Washington, DC.

Smith, D. Y., Shiles, E., and Inokuti, M., 1985, "The Optical Properties of Metallic Aluminum," in: *Handbook of Optical Constants of Solids*, Palik, E. D., ed., Academic Press, Orlando, FL.

Stagg, B. J., and Charalampopoulos, 1991, "Surface Roughness Effects on the Determination of Optical Properties of Materials by the Reflection Method," *Appl. Opt.*, Vol. 30, pp. 4113–4118.

van der Meulen, Y. J., and Hien, N. C., 1974, "Design and Operation of an Automated High Temperature Ellipsometer," *J. Opt. Soc. Amer.*, Vol. 64, pp. 804–811.

Zweidinger, D. T., Fox, R. M., Brodsky, J. S., Jung, T., and Lee, S., 1996, "Thermal Impedance Extraction for Bipolar Transistors," *IEEE Trans. Electron Devices*, Vol. 43, pp. 342–346.